

Energetics of phase transitions in homogeneous antiferromagnets

M. Hu,¹ M. A. Hofer,¹ and M. J. Donahue²

¹University of Colorado Boulder, Boulder, CO 80309, USA

²National Institute of Standards and Technology, Gaithersburg, MD 20899, USA

(*Electronic mail: michael.donahue@nist.gov)

(Dated: 17 August 2023)

Spatially uniform static phases in an antiferromagnet (AFM) at 0 K accessible by varying an external magnetic field along the anisotropy axis are investigated. Using the macrospin model, the energy contributions are comprised of the external field, effective anisotropy, and spatially homogeneous AFM exchange. The critical energy configurations are fully cataloged, and local energy concavity is used to identify stable states. Relative energy levels are taken into account to classify phase transitions. Phase diagrams for energetic stability and phase transitions are provided in terms of the strength of the applied field and the ratio between anisotropy and the AFM exchange. Two nonstandard critical energy states are identified as energy saddle points, so are not stable but function as energy barriers between multiple stable states. The results determine thermal switching rates and suggest interesting AFM textures and solitons.

Although antiferromagnets (AFMs) are known to be robust against perturbation by external magnetic fields, a series of magnetic phases will manifest in a bipartite AFM depending on the field magnitude and the material properties. These phases can be used to construct magnetic textures such as domain walls¹⁻⁴ and solitons.⁵⁻⁷ Understanding the full energy landscape is necessary to characterize thermally activated switching events. New optical measurement capabilities of AFMs⁸ open up the possibility of measuring novel magnetic textures. There have been continuing efforts to uncover all critical energy points as local energy minimum candidates and to understand the phase transition mechanisms. However, previous work either failed to compute the complete pool of critical energy points,⁹⁻¹³ restricted the possible degrees of freedom,¹⁴ or missed the local stability analysis.¹⁵ Moreover, unstable intermediate states have not been identified as the only saddle point energy barriers in phase transitions. In this letter, we present a theoretical investigation of all static, spatially uniform, critical energy points in a two-sublattice AFM with the external magnetic field applied along the anisotropy axis. All local energy minima, maxima, and saddle points are identified, the last marking energy barriers between energy minima. Several examples mapping typical AFM materials onto this framework are provided.

Using the macrospin model,^{16,17} the energy is composed of the applied field, effective anisotropy, and the spatially homogeneous AFM exchange. Both easy-axis and easy-plane anisotropy cases are considered. This model is simultaneously complex enough to include many phases yet remains tractable enough for a rigorous mathematical treatment. In the following discussions, a phase is considered to be energetically stable if it is a local energy minimum.^{18,19} It is further considered energetically preferred if it is also a global energy minimum. A phase transition takes place when the energetically preferred phase changes.^{17,18,20,21} We identify all possible phase transitions and discuss the implications on AFM magnetic textures involving stable phases and saddle points.

Without loss of generality, we let the anisotropy axis be \hat{z} and consider an external magnetic field of magnitude h_0 applied along the z -axis. The nondimensional energy for the spatially uniform two-sublattice macrospin model is given by

$$E = -h_0(\mathbf{m}_A \cdot \hat{z} + \mathbf{m}_B \cdot \hat{z}) + h_e \mathbf{m}_A \cdot \mathbf{m}_B - \frac{h_k}{2} \left[(\mathbf{m}_A \cdot \hat{z})^2 + (\mathbf{m}_B \cdot \hat{z})^2 \right], \quad (1)$$

where

$$\mathbf{m}_i = \frac{\mathbf{M}_i}{M_s} = (\sin \Theta_i \cos \Phi_i, \sin \Theta_i \sin \Phi_i, \cos \Theta_i), \quad i = A \text{ or } B, \quad (2)$$

is the magnetization vector normalized by the saturation magnetization M_s . The subscript A or B denotes the sublattice while $\Theta_i \in [0, \pi]$ is the polar angle, $\Phi_i \in [0, 2\pi]$ is the azimuthal angle, $i = A$ or B , $h_e > 0$ is the spatially homogeneous AFM exchange coefficient, and h_k is the effective anisotropy coefficient. When $h_k > 0$, anisotropy has the easy-axis \hat{z} . When $h_k < 0$, anisotropy is easy-plane with hard axis \hat{z} .

To find all critical energy points,²² we set

$$\left(\frac{\partial E}{\partial \Theta_A}, \frac{\partial E}{\partial \Theta_B}, \frac{\partial E}{\partial \Phi_A}, \frac{\partial E}{\partial \Phi_B} \right) = (0, 0, 0, 0). \quad (3)$$

Then, the necessary conditions for a critical energy point are

$$\Theta_A = 0 \text{ or } \pi, \text{ and } \Theta_B = 0 \text{ or } \pi, \quad (4)$$

or

$$|\Phi_A - \Phi_B| = \pi \text{ or } 0. \quad (5)$$

The former condition leads to two vacuum phases (so-called because Φ_A and Φ_B are undefined) as critical points: the AFM and FM phases listed in Table I. The schematics are shown in Figs. 1(a) and 1(b).

TABLE I. Vacuum critical energy points in an AFM.

Phase name	Phase configuration
AFM	$(\Theta_A, \Theta_B) = (0, \pi) \text{ or } (\pi, 0)$
FM	$\Theta_A = \Theta_B = 0 \text{ or } \pi$

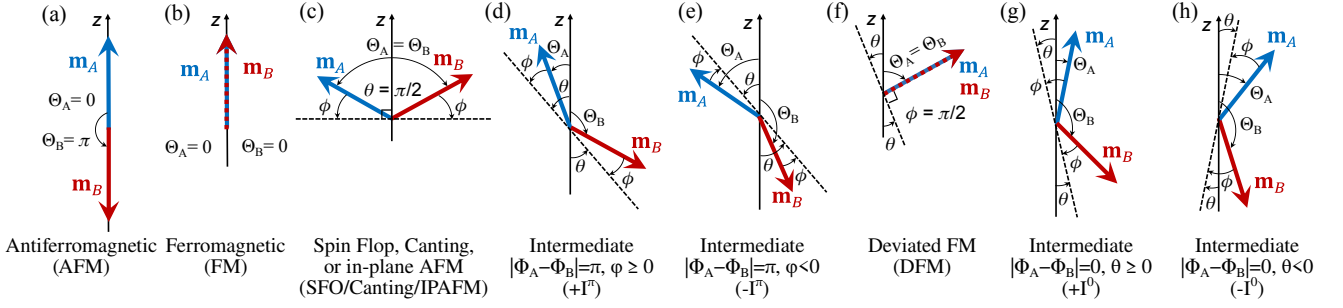


FIG. 1. Schematics for critical energy points. The Néel vector \mathbf{n} lies along the dotted blacked line. (a) AFM: $\Theta_A = 0$, $\Theta_B = \pi$. (b) Spin-up FM: $\Theta_A = \Theta_B = 0$. (c) SFO ($h_k > 0$) or canting ($h_k < 0$): $|\Phi_A - \Phi_B| = \pi$, $\Theta_A = \Theta_B$; IPAFM is canting with $\phi = 0$. (d) $+I^\pi$: $|\Phi_A - \Phi_B| = \pi$, $\Theta_A + \Theta_B \leq \pi$. (e) $-I^\pi$: $|\Phi_A - \Phi_B| = \pi$, $\Theta_A + \Theta_B > \pi$. (f) DFM: $\Phi_A - \Phi_B = 0$, $\Theta_A = \Theta_B$. (g) $+I^0$: $\Phi_A - \Phi_B = 0$, $\Theta_A + \Theta_B \leq \pi$. (h) $-I^0$: $\Phi_A - \Phi_B = 0$, $\Theta_A + \Theta_B > \pi$.

The condition (5) indicates that the two sublattice magnetization vectors are on the same plane perpendicular to the xy -plane. Without loss of generality, we let \mathbf{m}_A and \mathbf{m}_B lie in the xz -plane. To compute all non-vacuum critical points, we consider the Néel vector $\mathbf{n} = (\mathbf{m}_A - \mathbf{m}_B)/2$ and introduce

- θ : the angle between the z -axis and \mathbf{n} .
 - For $|\Phi_A - \Phi_B| = \pi$, $\theta \in [0, \pi/2]$.
 - For $\Phi_A - \Phi_B = 0$, $\theta \in [-\pi/2, \pi/2]$. If $\Theta_A + \Theta_B \leq \pi$, then $\theta \geq 0$, otherwise $\theta < 0$.
- ϕ : the angle between \mathbf{m}_A and \mathbf{n} .
 - For $|\Phi_A - \Phi_B| = \pi$, $\phi \in [-\pi/2, \pi/2]$. If $\Theta_A + \Theta_B \leq \pi$, then $\phi \geq 0$, otherwise $\phi < 0$.
 - For $\Phi_A - \Phi_B = 0$, $\phi \in [0, \pi/2]$.

The restrictions on θ and ϕ assume $\Theta_A \leq \Theta_B$ without loss of generality for the purpose of obtaining the mathematical definitions of the critical phases. The benefit of this coordinate system is that it characterizes the symmetry of \mathbf{m}_A and \mathbf{m}_B about the Néel vector \mathbf{n} , thus making the computation of critical points easier. To solve for critical energy points, we require

$$\left(\frac{\partial E}{\partial \theta}, \frac{\partial E}{\partial \phi} \right) = (0, 0). \quad (6)$$

For the $|\Phi_A - \Phi_B| = \pi$ case, we have

$$\theta = \frac{\pi}{2} + \frac{\Theta_A - \Theta_B}{2}, \quad \phi = \frac{\pi}{2} - \frac{\Theta_A + \Theta_B}{2}. \quad (7)$$

The non-vacuum critical energy points are the spin-flopped (SFO) phase when $h_k > 0$ or the canting phase when $h_k < 0$ (Fig. 1(c)), and two intermediate (I^π) phases: $+I^\pi$ phase when $\phi \geq 0$ (Fig. 1(d)) and $-I^\pi$ phase when $\phi < 0$ (Fig. 1(e)). Table II lists the mathematical definitions of all non-vacuum critical energy points by considering $h_0 \geq 0$ without loss of generality. The SFO and canting phases are well-studied in phase transitions.¹⁶ The SFO phase is achieved when the applied magnetic field fully compensates the easy-axis anisotropy, whereas the canting phase exhibits a balance between Zeeman

and AFM exchange energies. The $+I^\pi$ phase has been theoretically studied for a biaxial AFM.^{9,10,23} The name “intermediate” is inherited from Yamashita⁹ and is extended to other critical energy points whose spin configuration is between the AFM and SFO phases. Collectively, the intermediate phases are referred to as I^* phases in the rest of the paper.

When

$$h_0 > 2h_e - h_k \equiv h_{cr1}, \quad (8)$$

the Zeeman energy dominates the AFM exchange energy and therefore the SFO or canting phase saturates to the FM phase, imposing a field restriction for the existence of such phases. When $\theta = \pi/2$ and $\phi = 0$, the canting phase is referred to as the in-plane AFM (IPAFM) phase. The $\pm I^\pi$ phases are only defined on restricted regimes indicated in Table III. The critical fields bounding the existence of the $\pm I^\pi$ phases are

$$h_{cr2} \equiv (2h_e - h_k) \sqrt{\frac{h_k}{2h_e + h_k}}, \quad (9)$$

$$h_{cr3} \equiv \sqrt{h_k(2h_e + h_k)}.$$

We will show that the $\pm I^\pi$ phases are not energetically stable, but they determine energy barriers between multiple stable phases.

For the $\Phi_A - \Phi_B = 0$ case,

$$\theta = \frac{\pi}{2} - \frac{\Theta_A + \Theta_B}{2}, \quad \phi = \frac{\pi}{2} + \frac{\Theta_A - \Theta_B}{2}. \quad (10)$$

The non-vacuum critical energy points are the deviated FM (DFM) phase (Fig. 1(f)), first identified by Yamashita,⁹ and two intermediate ($\pm I^0$) phases: $+I^0$ phase with $\theta \geq 0$ (Fig. 1(g)) and $-I^0$ phase with $\theta < 0$ (Fig. 1(h)). The mathematical definitions of all non-vacuum critical points are listed in Table II. When

$$h_0 \geq h_k \equiv h_{cr4}, \quad (11)$$

the DFM phase saturates to the FM phase, imposing a field restriction for the existence of the DFM phase. Although the DFM phase was ruled out in phase transitions by Li¹⁵ based on its high energy relative to other critical energy points, we

TABLE II. Non-vacuum critical energy points in an AFM.

Phase name	Phase configuration
SFO ($h_k > 0$) or canting ($h_k < 0$)	$\theta = \pi/2, \phi = \arcsin\left(\frac{h_0}{2h_e - h_k}\right)$
DFM	$\theta = -\arcsin(h_0/h_k), \phi = \pi/2$
$+I^\pi$ ($\phi \geq 0$), $+I^0$ ($\theta \geq 0$)	$\theta = \arctan\left(\frac{\sqrt{[2h_e + h_k - h_0\sqrt{(2h_e + h_k)/h_k}]} / \sqrt{[-2h_e + h_k + h_0\sqrt{(2h_e + h_k)/h_k}]}}{\sqrt{[2h_e + h_k - h_0\sqrt{(2h_e + h_k)/h_k}]} / \sqrt{[2h_e + h_k + h_0\sqrt{(2h_e + h_k)/h_k}]}}\right),$ $\phi = \arctan\left(\frac{\sqrt{[2h_e + h_k - h_0\sqrt{(2h_e + h_k)/h_k}]} / \sqrt{[-2h_e + h_k + h_0\sqrt{(2h_e + h_k)/h_k}]}}{\sqrt{[2h_e + h_k - h_0\sqrt{(2h_e + h_k)/h_k}]} / \sqrt{[2h_e + h_k + h_0\sqrt{(2h_e + h_k)/h_k}]}}\right)$
$-I^\pi$ ($\phi < 0$, upper sign), $-I^0$ ($\theta < 0$, lower sign)	$\theta = \pm \arctan\left(\frac{\sqrt{[2h_e + h_k + h_0\sqrt{(2h_e + h_k)/h_k}]} / \sqrt{[-2h_e + h_k - h_0\sqrt{(2h_e + h_k)/h_k}]}}{\sqrt{[2h_e + h_k + h_0\sqrt{(2h_e + h_k)/h_k}]} / \sqrt{[2h_e + h_k - h_0\sqrt{(2h_e + h_k)/h_k}]}}\right),$ $\phi = \mp \arctan\left(\frac{\sqrt{[2h_e + h_k + h_0\sqrt{(2h_e + h_k)/h_k}]} / \sqrt{[-2h_e + h_k - h_0\sqrt{(2h_e + h_k)/h_k}]}}{\sqrt{[2h_e + h_k + h_0\sqrt{(2h_e + h_k)/h_k}]} / \sqrt{[2h_e + h_k - h_0\sqrt{(2h_e + h_k)/h_k}]}}\right)$

TABLE III. Existence conditions for I^* phases.

Phase name	Parameter regime	Existence conditions
$+I^\pi$ and $+I^0$	$h_k > 0$	<ol style="list-style-type: none"> $h_k < 2h_e$ and $h_{cr2} \leq h_0 \leq h_{cr3}$ $h_k \geq 2h_e$ and $h_0 \leq h_{cr3}$
	$h_k < 0$	<ol style="list-style-type: none"> $h_k \leq -2h_e$ and $h_0 \leq h_{cr3}$
$-I^\pi$ and $-I^0$	$h_k > 0$	<ol style="list-style-type: none"> $h_k \geq 2h_e$ and $h_0 \leq -h_{cr2}$
	$h_k < 0$	<ol style="list-style-type: none"> $h_k \leq -2h_e$ and $h_0 \leq h_{cr3}$

will show that it is never energetically stable. The existence conditions for the $\pm I^0$ phases are the same as those for the $\pm I^\pi$ phases, respectively, as indicated in Table III.

We study the stability of the identified critical energy points using the Hessian test.²² To consider all vacuum and non-vacuum phases at the same time, we return to polar coordinates and compute the Hessian matrix for the energy (1) with respect to Θ_A , Θ_B , and $\Phi_A - \Phi_B$, a total of three degrees of freedom to fully characterize the local energy concavity. An incomplete stability analysis using the Hessian approach was adopted by Yamashita⁹ because the analysis was restricted to variations in only Θ_A and Θ_B . Here we incorporate one additional degree of freedom by allowing for changes in $\Phi_A - \Phi_B$ because E is invariant to simultaneous rotations of \mathbf{m}_A and \mathbf{m}_B about $\hat{\mathbf{z}}$. The necessary condition for a local energy minimum is that all eigenvalues of the Hessian matrix must be

non-negative.²⁴ When all the eigenvalues of the Hessian matrix are non-positive, then the state is a local energy maximum. When there exist both positive and negative eigenvalues, then the state is a saddle point. Saddle points determine the lowest energy required for the transition from one local minimum to another local minimum, i.e., they determine an energy barrier. The combination of the gradient and Hessian tests provides necessary and sufficient conditions to classify local extrema. Considering all possible energetic degrees of freedom, we are able to exhaustively identify all energy extrema. This approach can be extended to other energy landscapes by symmetry breaking (canted applied field or biaxial anisotropy) necessitating four degrees of freedom ($\theta, \phi, \Phi_A, \Phi_B$).

TABLE IV. Stability regime for critical energy points.

Parameter regime	Phase name	Stable field interval	
$h_k > 0$	$h_k < 2h_e$	AFM	$0 \leq h_0 \leq h_{cr3}$
		SFO	$h_{cr2} \leq h_0 \leq h_{cr1}$
		FM, spin-up	$h_0 \geq h_{cr1}$
	$h_k \geq 2h_e$	AFM	$0 \leq h_0 \leq h_{cr3}$
		FM, spin-up	$h_0 \geq h_{cr1}$
		FM, spin-down	$h_0 \leq -h_{cr1}$
$h_k < 0$	IPAFM	$h_0 = 0$	
	Canting	$0 < h_0 \leq h_{cr1}$	
	FM, spin-up	$h_0 \geq h_{cr1}$	

The stability regimes when $h_0 \geq 0$ are plotted in Fig. 2(a) in terms of the scaled anisotropy coefficient and applied field

$$\begin{aligned} \bar{h}_k &= h_k/h_e, \\ \bar{h}_0 &= h_0/h_e. \end{aligned} \quad (12)$$

The stability regimes are also listed in Table IV. When $h_k > 0$, the only local minima are the AFM, SFO, and FM phases. The $\pm I^\pi$ and $\pm I^0$ phases are always saddles; the DFM phase is always a local maximum. When $h_k < 0$, the candidate critical points for phase transitions are the IPAFM phase, the canting phase, and the FM phase. The $\pm I^\pi$, $\pm I^0$, and DFM phases

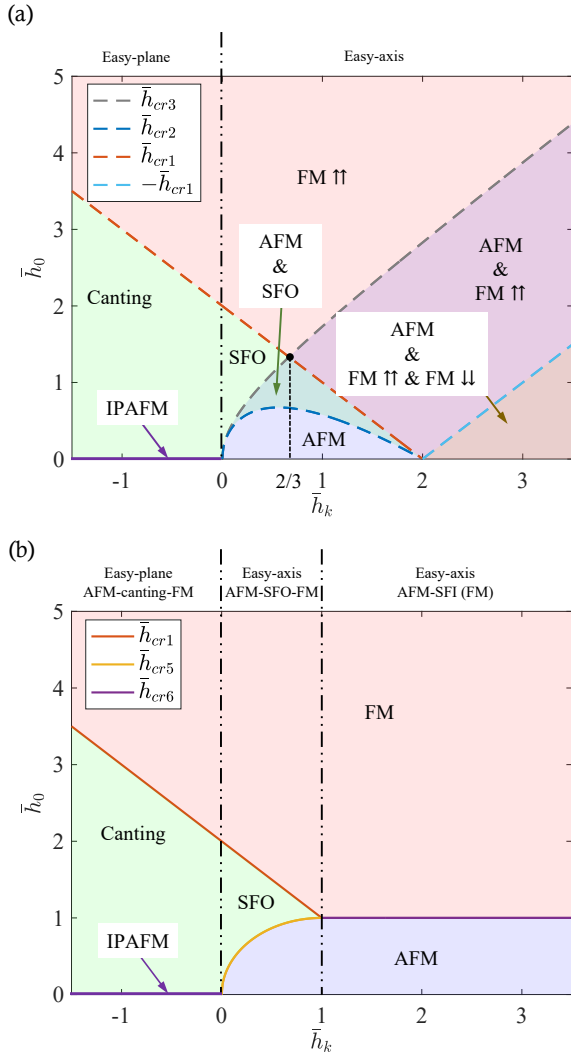


FIG. 2. Phase diagram for (a) energetic stability (local energy minimum) and (b) energetically preferred (global energy minimum) phase regions. All parameters and fields are scaled by h_e , denoted with a bar on top.

are always saddles. While two of the eigenvalues of the DFM phase are both positive or have opposite signs, the third eigenvalue obtained from variations in $\Phi_A - \Phi_B$ is always negative, decisively ruling out the possibility of a stable DFM phase. There exist overlapping regions where two or more critical energy phases are stable. In Fig. 2(a), bistability and tristability regions are indicated.

The critical fields bounding the existence of the I^* phases coincide with those bounding the stability of some critical energy points. When $0 < h_k < 2h_e$, the lower h_{cr2} and upper h_{cr3} bounds for the existence of $+I^\pi$ and $+I^0$ phases are the lower stability bound for the SFO phase and the upper stability bound for the AFM phase, respectively. If further $h_k \leq 2h_e/3$, the $+I^\pi$ and $+I^0$ phases can exist and are always saddle points precisely in the bistability region for AFM and SFO phases. If $2h_e/3 \leq h_k \leq 2h_e$, the $+I^\pi$ and $+I^0$ phases can exist as saddle points in the bistability region of the AFM and SFO phases

TABLE V. Summary of lowest-energy critical phases.

Parameter regime	Phase name	Lowest energy field interval
$h_k > 0$	AFM	$0 \leq h_0 \leq h_{cr5}$
	SFO	$h_{cr5} \leq h_0 \leq h_{cr1}$
	FM, spin-up	$h_0 \geq h_{cr1}$
	AFM	$0 \leq h_0 \leq h_{cr6}$
$h_k < 0$	FM, spin-up	$h_0 \geq h_{cr6}$
	IPAFM	$h_0 = 0$
	Canting	$0 < h_0 \leq h_{cr1}$
	FM, spin-up	$h_0 \geq h_{cr1}$

and some part of the bistability region of the AFM and spin-up FM phases. In addition, the existence regime of the $-I^\pi$ and $-I^0$ saddle points lies entirely in the tristability region of the AFM, spin-up FM, and spin-down FM phases when $h_k > 0$.

To identify phase transitions, we evaluate the energy of each critical energy phase. The lowest critical energy points are summarized in Table V where

$$h_{cr5} \equiv \sqrt{h_k(2h_e - h_k)}, \quad (13)$$

$$h_{cr6} \equiv h_e.$$

When $h_k > 0$, the SFO phase transition is found to only be possible when $h_k < h_e$. When $h_k \geq h_e$, the spin-flip (SFI) transition from the AFM to FM phase takes place. Thus, the energetically stable region of the SFO phase is larger than the energetically preferred region. This indicates that, even when $E_{SFO} > E_{AFM}$, the SFO phase may be achieved in the bistability region. The same argument applies to the AFM and FM phases in their bistability and tristability regions when $h_k > 0$. Combining the stability analysis and the lowest energy calculation, we obtain the energetically preferred phases as global energy minima shown in Fig. 2(b).

To apply Fig. 2 in a realistic setting, we list a few AFM materials and discuss the accessible phase transitions. Transition metal oxides, such as NiO and MnO, are examples of easy-plane AFMs. For NiO, the easy-plane anisotropy field is $H_A = -505$ kA/m and AFM exchange field is $H_E = 771$ MA/m,¹⁷ giving $\bar{h}_k = -6.56 \times 10^{-4}$. Examples of easy-axis AFMs with stronger AFM exchange than anisotropy are fluorides such as MnF₂ and FeF₂. For MnF₂, the easy-axis anisotropy field is $H_A = 653$ kA/m and the AFM exchange field is $H_E = 41.9$ MA/m,¹⁷ giving $\bar{h}_k = 0.0156 < 1$. According to Fig. 2(b), the SFO transition will take place when the applied magnetic field along the easy axis exceeds $h_{cr5} = \sqrt{h_k(2h_e - h_k)}$, in agreement with the critical transition field in Rezende et al.¹⁷ Moreover, because $\bar{h}_k = 0.0156 < 2/3$, only AFM-SFO bistability will exist when $h_{cr2} < h_0 < h_{cr3}$. For easy-axis AFMs with stronger anisotropy than AFM exchange, a well-studied material is FeCl₂,^{25,26} which has easy-axis anisotropy field $H_A = 13.5$ MA/m and AFM exchange field is $H_E = 867$ kA/m, yielding $\bar{h}_k = 15.6 > 1$. Both the material parameter coefficient, $\bar{h}_k \geq 1$, and the critical field for the SFI transition, $\bar{h}_{cr6} = 1$, agree with the results presented in Jacobs and Lawrence²⁵ at 0 K. According to Fig. 2(a), since $\bar{h}_k = 15.6 > 2$, bistability and tristability regimes are accessible.

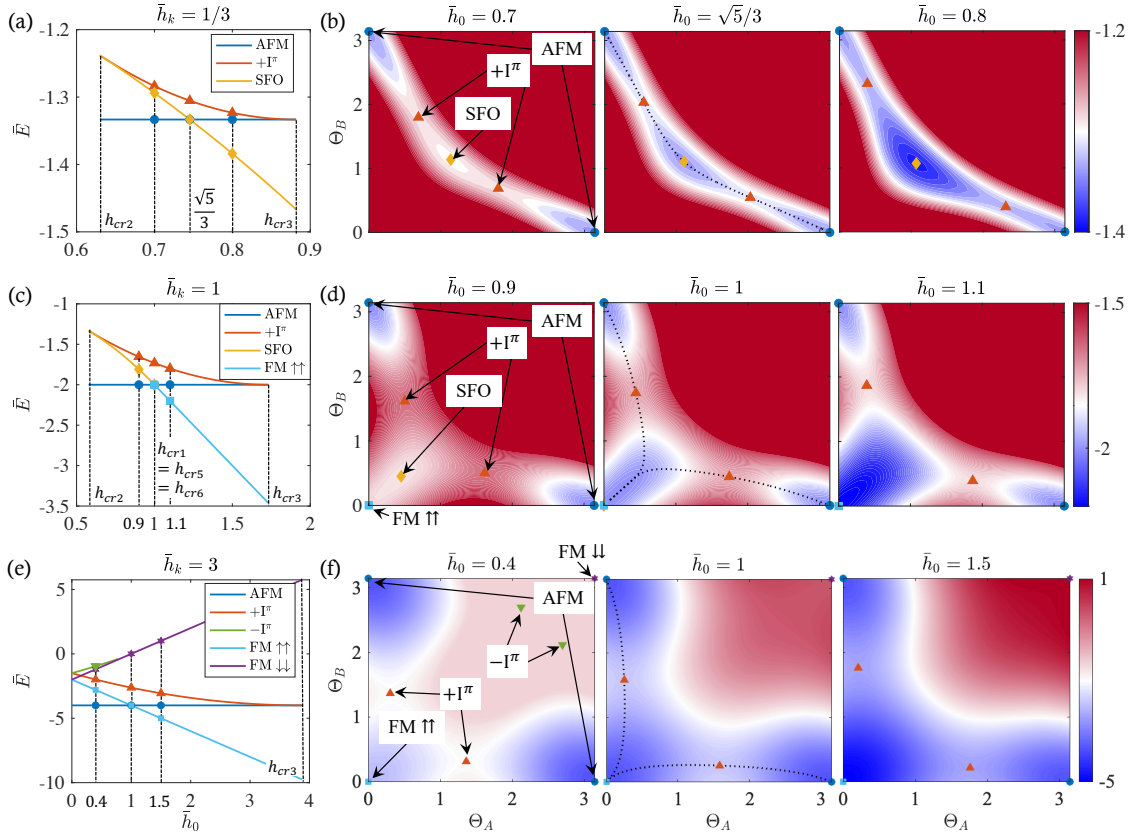


FIG. 3. Energetics of critical energy points when $|\Phi_A - \Phi_B| = \pi$. Energy magnitudes of critical energy points are plotted when (a) $\bar{h}_k = 1/3$, (c) $\bar{h}_k = 1$, and (e) $\bar{h}_k = 3$. The vertical axis is the scaled energy $\bar{E} = E/h_e$, the horizontal axis is the scaled applied field \bar{h}_0 . Energy contours are plotted when (b) $\bar{h}_k = 1/3$, (d) $\bar{h}_k = 1$, and (f) $\bar{h}_k = 3$. The vertical axis is Θ_B , the horizontal axis is Θ_A , and the color bar on the far right indicates \bar{E} . The black dotted curves in the energy contour plots are the lowest energy path connecting global energy minima through the $+I^\pi$ saddle point.

While the I^* phases are never energetically stable, they do play a role in phase transitions. We focus on the $|\Phi_A - \Phi_B| = \pi$ case and thus only $+I^\pi$ and $-I^\pi$ are relevant. Fig. 3 plots the energy magnitudes and energy contours with $|\Phi_A - \Phi_B| = \pi$ for several values of \bar{h}_k : $\bar{h}_k = 1/3$, 1, and 3 in the top, middle, and bottom rows, respectively. In Fig. 3(a) when $\bar{h}_k = 1/3$, the energetics are investigated in the AFM-SFO bistability region. In the contour plots for different \bar{h}_0 in Fig. 3(b), the AFM and SFO phases are local energy minima while the $+I^\pi$ phase is the saddle point in between, serving as the energy barrier between the AFM and SFO phases. Similarly, in Figs. 3(c) and 3(d) when $\bar{h}_k = 1$, the $+I^\pi$ phase is a saddle point that serves as the energy barrier between the AFM and SFO phases. The subtlety here is that when the AFM and SFO phases have the same energy (at $\bar{h}_0 = 1$), the SFO phase saturates to the spin-up FM phase (lower left corner in Fig. 3(d)). Thus, when $\bar{h}_k \geq 1$, the phase transition that takes place is the SFI transition. In Figs. 3(e) and 3(f) when $\bar{h}_k = 3$, the $+I^\pi$ phase serves as the energy barrier between the AFM and spin-up FM phases. When $\bar{h}_0 = 0.4$, the spin-down FM phase is a local energy minimum (upper right corner in Fig. 3(f)), although very shallow, and the $-I^\pi$ phase is a saddle point. Thus, the $-I^\pi$ phase functions as the energy barrier between the AFM and

spin-down FM phases in the tristability region of the AFM, spin-up FM, and spin-down FM phases. Hence, the $+I^\pi$ phase is the energy barrier between the AFM and SFO phases and between the AFM and FM phases in the bistability and tristability regions. The $-I^\pi$ phase is the energy barrier between the AFM and FM phases in the tristability region. The energy barrier heights when $h_k > 0$ are evaluated to be

$$E_{+I^\pi} = \frac{h_0^2 - h_k^2 - 2h_0\sqrt{h_k(2h_e + h_k)}}{2h_k},$$

$$E_{-I^\pi} = \frac{2h_0\sqrt{h_0^2 + 2h_e h_k + h_k^2} + 2h_0\sqrt{h_k(2h_e + h_k)} - h_0^2 - h_k^2}{2h_k}. \quad (14)$$

The coexistence of multiple energetically stable phases suggests (1) possible spatial transitions between energy minima if weak spatially inhomogeneous exchange interactions are included, and (2) thermally activated switching between stable states if thermal fluctuations are present. The energy barrier in both cases is determined by the saddle points. Taking the $+I^\pi$ saddle point as an example, we adiabatically trace the steepest energy descent paths between (1) the AFM and SFO phases in the AFM-SFO bistability region, and (2) the AFM and FM phases in the AFM-FM bistability region. These low-

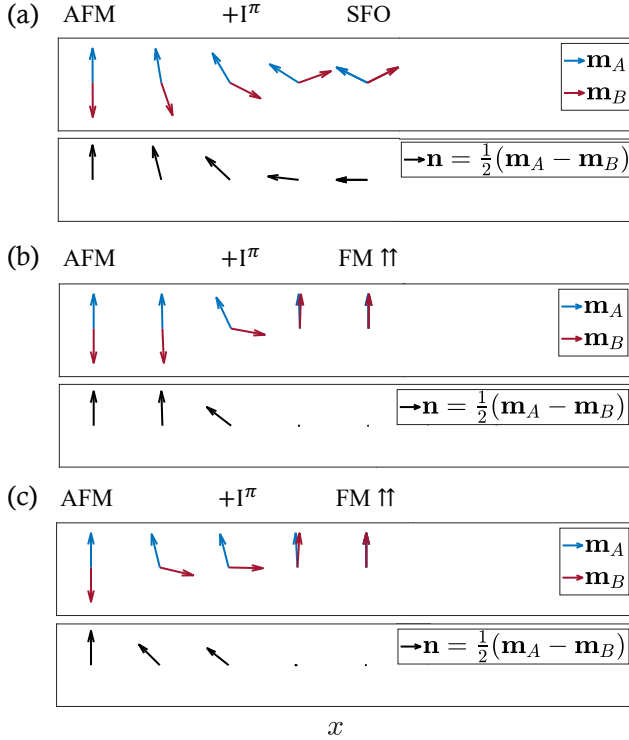


FIG. 4. Illustrations of AFM domain walls constructed from pairs of energetically stable phases that are connected by following the steepest energy descent paths from an energy saddle point. (a) $\tilde{h}_k = 1/3$ and $\tilde{h}_0 = \sqrt{5}/3$; (b) $\tilde{h}_k = 1$ and $\tilde{h}_0 = 1$; (c) $\tilde{h}_k = 3$ and $\tilde{h}_0 = 1$.

est energy paths are plotted in Figs. 3(b), 3(d), and 3(f) when the local energy minima have the same energy. Illustrations of AFM domain walls constructed in this manner are provided in Fig. 4. Figure 4(a) plots the spatial transition from the AFM phase to the SFO phase. If the end SFO phase further transitions back to the beginning AFM phase through the $+I^\pi$ phase, then we obtain a soliton. Similarly, spatial transitions between the AFM and FM phases can be constructed with illustrations provided in Figs. 4(b) and 4(c). If thermal fluctuations are present, the steepest descent paths we trace in Fig. 3 are the dynamic trajectories with the highest probability²⁷ for a thermally induced switching event due to weak thermal noise. According to Kramers' theory,²⁸ the thermally activated transition rate is

$$\tau^{-1} \sim \exp(-U/k_B T), \text{ when } k_B T \ll U, \quad (15)$$

where U is the energy barrier determined by the saddle points, k_B is the Boltzmann constant, and T is the temperature.

In conclusion, we provide phase diagrams in terms of the applied magnetic field and identify the material parameter regimes for energetically stable and energetically preferred phases in a static, spatially homogeneous AFM at 0 K. All possible phase transitions are exhaustively identified by leveraging both local energy concavity and relative energy magni-

tudes. Using the macrospin model, a complete classification of the existence and energetic stability of all critical energy points is achieved. For the nonstandard I^* and DFM phases, our analysis demonstrates that they are never energetically stable. Moreover, the $+I^\pi$ phase is explicitly identified to be the energy barrier during SFO and SFI transitions. The $-I^\pi$ phase is the energy barrier between the AFM and FM phases in the tristability region. Our thorough study of the energy landscape provides theoretical guidance for constructing spatial magnetic textures, thermally activated switching, and the appropriate material parameter regime for them.

ACKNOWLEDGMENTS

M. Hu would like to acknowledge support from the National Institute of Standards and Technology Professional Research Experience Program.

- ¹A. C. Swaving and R. A. Duine, "Current-induced torques in continuous antiferromagnetic textures," *Phys. Rev. B* **83**, 054428 (2011).
- ²E. G. Tveten, A. Qaiumzadeh, O. A. Tretiakov, and A. Brataas, "Staggered dynamics in antiferromagnets by collective coordinates," *Phys. Rev. Lett.* **110**, 127208 (2013).
- ³O. Gomonay, T. Jungwirth, and J. Sinova, "High antiferromagnetic domain wall velocity induced by Néel spin-orbit torques," *Phys. Rev. Lett.* **117**, 017202 (2016).
- ⁴D. R. Rodrigues, K. Everschor-Sitte, O. A. Tretiakov, J. Sinova, and A. Abanov, "Spin texture motion in antiferromagnetic and ferromagnetic nanowires," *Phys. Rev. B* **95**, 174408 (2017).
- ⁵H. J. Mikeska, "Non-linear dynamics of classical one-dimensional antiferromagnets," *Journal of Physics C: Solid State Physics* **13**, 2913–2923 (1980).
- ⁶A. M. Kosevich, B. Ivanov, and A. Kovalev, "Magnetic solitons," *Physics Reports* **194**, 117–238 (1990).
- ⁷E. Galkina and B. Ivanov, "Dynamic solitons in antiferromagnets," *Low Temperature Physics* **44**, 618–633 (2018).
- ⁸P. Němec, M. Fiebig, T. Kampfrath, and A. V. Kimel, "Antiferromagnetic opto-spintronics," *Nature Physics* **14**, 229–241 (2018).
- ⁹N. Yamashita, "Field induced phase transitions in uniaxial antiferromagnets," *J. Phys. Soc. Jpn.* **32**, 610–615 (1972).
- ¹⁰G. Kozłowski, "The stability of the field-induced magnetic phases of a uniaxial antiferromagnet at zero temperature," *Physics Letters A* **35**, 359–360 (1971).
- ¹¹U. K. Röbller and A. N. Bogdanov, "Magnetic phase diagrams for models of synthetic antiferromagnets," *J. Appl. Phys.* **101**, 09D105 (2007).
- ¹²D. C. Worledge, "Magnetic phase diagram of two identical coupled nanomagnets," *Appl. Phys. Lett.* **84**, 2847–2849 (2004).
- ¹³A. N. Bogdanov and U. K. Röbller, "Instabilities of switching processes in synthetic antiferromagnets," *Appl. Phys. Lett.* **89**, 163109 (2006).
- ¹⁴A.-V. Plamadă, D. Cimpoesu, and A. Stancu, "Activation energy and switching behavior of two interacting identical magnetic particles," *Appl. Phys. Lett.* **96**, 122505 (2010).
- ¹⁵H.-F. Li, "Possible ground states and parallel magnetic-field-driven phase transitions of collinear antiferromagnets," *npj Comput. Mater.* **2**, 16032 (2016).
- ¹⁶V. Baltz, A. Manchon, M. Tsui, T. Moriyama, T. Ono, and Y. Tserkovnyak, "Antiferromagnetic spintronics," *Rev. Mod. Phys.* **90**, 015005 (2018).
- ¹⁷S. M. Rezende, A. Azevedo, and R. L. Rodríguez-Suárez, "Introduction to antiferromagnetic magnons," *J. Appl. Phys.* **126**, 151101 (2019).
- ¹⁸F. B. Anderson and H. B. Callen, "Statistical mechanics and field-induced phase transitions of the Heisenberg antiferromagnet," *Phys. Rev.* **136**, A1068–A1087 (1964).
- ¹⁹W. Yung-Li and H. B. Callen, "Spin waves in the spin-flop phase of an antiferromagnet, and metastability of the spin-flop transition," *J. Phys. Chem. Solids* **25**, 1459–1463 (1964).

- ²⁰R. L. Carlin and A. van Duynveldt, "Special topics: Spin-flop, metamagnetism, ferrimagnetism and canting," in *Magnetic Properties of Transition Metal Compounds* (Springer, 1977) pp. 172–194.
- ²¹N. Ntallis and K. Efthimiadis, "Micromagnetic simulation of an antiferromagnetic particle," *Computational Materials Science* **97**, 42–47 (2015).
- ²²J. D. Fehribach, "Multivariable and vector calculus," in *Multivariable and Vector Calculus* (De Gruyter, 2020).
- ²³C. C. Becerra and L. G. Ferreira, "Phase transitions in uniaxial antiferromagnets," *J. Phys. Soc. Jpn.* **37**, 951–955 (1974).
- ²⁴R. B. Bapat, "Eigenvalues and positive definite matrices," in *Linear Algebra and Linear Models* (Springer London, London, 2012) pp. 21–29.
- ²⁵I. S. Jacobs and P. E. Lawrence, "Metamagnetic phase transitions and hysteresis in FeCl₂," *Physical Review* **164**, 866 (1967).
- ²⁶R. J. Birgeneau, W. B. Yelon, E. Cohen, and J. Makovsky, "Magnetic properties of FeCl₂ in zero field. I. Excitations," *Physical Review B* **5**, 2607 (1972).
- ²⁷H. Touchette, "The large deviation approach to statistical mechanics," *Physics Reports* **478**, 1–69 (2009).
- ²⁸P. Hänggi, P. Talkner, and M. Borkovec, "Reaction-rate theory: Fifty years after Kramers," *Reviews of Modern Physics* **62**, 251 (1990).